Soft Matter

PAPER

View Article Online
View Journal | View Issue

Cite this: *Soft Matter*, 2019, **15**, 2439

Migration of ferrofluid droplets in shear flow under a uniform magnetic field†

Jie Zhang,[a] Md. Rifat Hassan,[a] Bhargav Rallabandi[b] and Cheng Wang *[a]

Received 14th December 2018,
Accepted 13th February 2019

DOI: 10.1039/c8sm02522c

rsc.li/soft-matter-journal

Manipulation of droplets based on physical properties (*e.g.*, size, interfacial tension, electrical, and mechanical properties) is a critical step in droplet microfluidics. Manipulations based on magnetic fields have several benefits compared to other active methods. While traditional magnetic manipulations require spatially inhomogeneous fields to apply forces, the fast spatial decay of the magnetic field strength from the source makes these techniques difficult to scale up. In this work, we report the observation of lateral migration of ferrofluid (or magnetic) droplets under the combined action of a uniform magnetic field and a pressure-driven flow in a microchannel. While the uniform magnetic field exerts negligible net force on the droplet, the Maxwell stresses deform the droplet to achieve elongated shapes and modulate the orientation relative to the fluid flow. Hydrodynamic interactions between the droplets and the channel walls result in a directional lateral migration. We experimentally study the effects of field strength and direction, and interfacial tension, and use analytical and numerical modeling to understand the lateral migration mechanism.

1 Introduction

Droplet microfluidics has emerged as a powerful technology on lab-on-a-chip platforms for high-throughput screening of chemical and biological assays.[1–3] Dispersed in a continuous phase, individual droplets often encapsulate chemical or biological samples (*e.g.*, cells, DNA, proteins, and bacteria), serve as miniaturized reactors, and allow biological and chemical reactions inside individual micro-droplets.[4] The large surface to volume ratio leads to significantly enhanced mass and heat transfer and bio-/chemical reactions. Furthermore, the high-throughput nature enables a vast number of assays in parallel, thereby drastically improving the accuracy of the results.

Manipulation, *e.g.*, sorting, of the droplets based on their contents or properties is often a critical step in a chemical or biological assay. Droplets can be sorted using passive or active methods. Passive methods are based on hydrodynamic features, such as geometry and fluid properties, to manipulate the droplets.[5–10] For passive methods to be effective, a complex geometry is usually employed or a particular fluid such as a viscoelastic fluid is used as a buffer, which places some limitations on lab-on-a-chip applications. Active methods employ external fields,[11] such as electric,[12–24] acoustic,[25–30] or magnetic forces,[31–39] to manipulate droplets. Among the various active methods, magnetic methods have several distinctive advantages, such as low or no heat generation, simple implementation and contactless control, and have, thus, received increasing attention over the last few years.[40]

Ferrofluids are colloidal suspensions composed of superparamagnetic nanoparticles. Magnetic particles in a ferrofluid commonly have a size of around 10 nm and are coated with surfactant to stabilize them and prevent agglomeration. Due to their ability to be controlled by external magnetic fields, ferrofluids have been widely used in applications in mechanical and biomedical fields.[41–43] Some typical applications of ferrofluids in mircofluidics include microvalves,[44] micropumps,[45] magnetic drug targeting[46] and magnetic separations of cells.[47] More recently in droplet microfluidics, ferrofluid droplets have been used to encapsulate cells for culturing and sorting[48] purposes, owing to their bio-compability and ease of manipulation with magnetic fields.

Traditional magnetic manipulation of ferrofluid droplets mainly relies on magnetic forces acting on the droplets. Assuming small field variations over the droplet volume V_p, the magnetic force is[49] $\mathbf{F}_m = \mu_0 V_p[(\mathbf{M}_p - \mathbf{M}_f)\cdot\nabla]\mathbf{H}$, where μ_0 is the magnetic permeability of vacuum, $\mathbf{H}$ is the magnetic field, and, $\mathbf{M}_p$ and $\mathbf{M}_f$ denote the magnetization of the droplet and the fluid respectively. Selective manipulation of droplets is possible based on the susceptibility contrast between the droplet and the surrounding phase, and the droplet size (or volume). A number of groups have utilized the magnetic force approach for various applications, including sorting of microalgae encapsulated in ferrofluid droplets,[48] on-chip manipulation of ferrofluid droplets in water[33]

[a] *Department of Mechanical and Aerospace Engineering, Missouri University of Science and Technology, 400 W. 13th St., Rolla, Missouri, 65409, USA. E-mail: wancheng@mst.edu; Fax: +1-573-341-4607; Tel: +1-573-341-4636*
[b] *Department of Mechanical Engineering, University of California, Riverside, California 92521, USA*

† Electronic supplementary information (ESI) available. See DOI: 10.1039/c8sm02522c

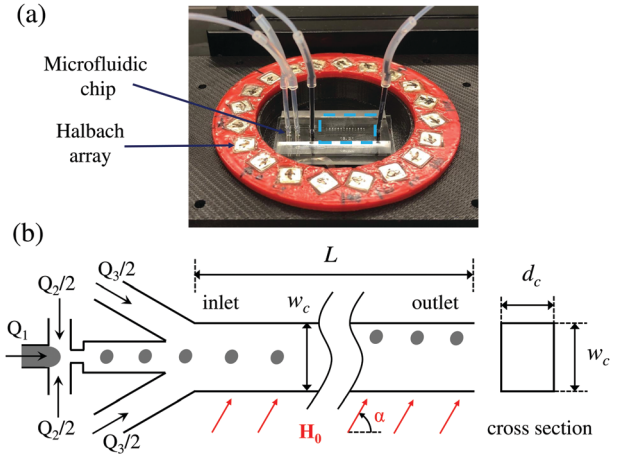

Fig. 1 (a) Photo of the microfluidic chip located in a uniform magnetic field. (b) Schematic showing the dimensions of the microchannel.

or water droplets in ferrofluid,[35] and selective distribution of water-in-magnetic-fluid droplets in curved channels.[36] However, due to the fast decay of magnetic fields with distance from the source,[50] magnetic sources need to be placed in proximity to the droplets in order to exert sufficient influence on the droplets. Often permanent magnets have to be placed near the microfluidic channels,[33,35,36,48] further making the scaling up of magnetic manipulation difficult.

In this work, we propose and demonstrate experimentally a simple and novel droplet manipulation technique by using a uniform magnetic field. In this method, while the uniform magnetic field does not directly exert magnetic forces on the droplets, it modulates the deformation of the micro-droplets, which consequently leads to a net lift force and lateral migrations of the droplets in shear flows. Although deformation of a ferrofluid droplet in a uniform magnetic field has been well studied[51] in an unbounded quiescent fluid, previous studies have not proposed the utilization of deformed shape to control droplet migration. In this work, we explain the cross-stream migration using a hydrodynamic theory involving the interaction of the deformed droplet's stresslet field with the walls of the channel. We then also use numerical simulations, based on the level-set method, to better understand the magnetic and flow fields around the droplets and confirm the migration mechanism.

2 Experiment

Fig. 1(a) shows the microfluidic chip placed in a uniform magnetic field with strength H_0 and direction α, which is generated by a Halbach array.[52] The microfluidic chip was fabricated with polydimethylsiloxane (PDMS) using a previously reported soft-lithography method.[53] The width, depth and length of the main microchannel are w_c = 800 μm, d_c = 70 μm, and $L \approx$ 13 000 μm as shown in Fig. 1(b). Three different sets of Halbach arrays were designed to generate the uniform magnetic fields, which consisted of 20 cuboid permanent 0.25″ × 0.25″ × 0.25″, 0.25″ × 0.25″ × 0.5″ or 0.25″ × 0.25″ × 1″ magnets (K&J Magnetics, Inc.). The details of the design and test of the uniform magnetic field can be seen in the ESI† of the previous reported work.[54] The magnitudes of these magnetic fields within the central region were measured as $H_0 \approx$ 18 000, 35 000 and 60 000 A m^{-1} using a gaussmeter. The droplet is generated by a flow-focusing configuration upstream, as shown in Fig. 1(b). Water-based ferrofluid (EMG 304, Ferrotec Corp.) is the dispersed phase, with density $\rho_f = 1.24 \times 10^3$ kg m^{-3}, viscosity $\eta_f = 5 \times 10^{-3}$ Pa s and an initial magnetic susceptibility (*i.e.* at small field strength) $\chi_f = 5.03$. Olive oil is used as the continuous phase and buffer fluid, with density $\rho_o = 0.92 \times 10^3$ kg m^{-3}, viscosity $\eta_o = 78 \times 10^{-3}$ Pa s, and magnetic susceptibility $\chi_o \approx 0$. Three different olive oil solutions were prepared by adding 0.125 wt%, 0.25 wt%, and 0.375 wt% of surfactant SPAN 80 (Sigma-Aldrich, USA) to vary the interfaical tension. The corresponding oil–ferrofluid interfacial tensions were measured as 5.86 ± 0.19, 4.31 ± 0.22 and 2.52 ± 0.22 mN m^{-1} using the pendant droplet method.[55] Three syringe pumps (KDS Scientific) were used to control the flow rates of the inlets. The flow rates of the dispersed phase (*i.e.*, ferrofluid), the continuous phase and the buffer flow are Q_1 = 0.15 μL min^{-1}, Q_2 = 4 μL min^{-1} and Q_3 = 6 μL min^{-1}. At these flow rates, the mean fluid speed is $\bar{u} \approx$ 3 mm s^{-1} and the corresponding Reynolds number in the main channel is Re ≈ 0.028. The trajectories of the ferrofluid droplets were recorded using an inverted microscope (IX73, Olympus) with a high-speed CCD camera (Phantom Miro M310, Vision Research). Custom MATLAB codes were written to analyze the centroid position and shape (including deformation and orientation) of the droplets from the recorded videos.

3 Results and discussion

3.1 Effect of direction of the magnetic field

Fig. 2 shows the images of droplets at the inlet and the outlet and the corresponding probability distributions of the droplet centroid in the y direction. In this experiment, the oil–ferrofluid interfacial tension is σ = 4.31 ± 0.22 mN m^{-1}. The average radius of the undeformed droplet is R_0 = 60.76 μm. The droplets are generated upstream and enter along the center-line of the channel. As can be seen from Fig. 2(a1)–(a3), there is negligible deformation and almost zero net lateral migration in the cross-stream direction (*i.e.*, y direction) when no magnetic field is applied (H_0 = 0). Since the Reynolds number is small (Re ≈ 0.028 ≪ 1), inertial effects are negligible. According to previous theoretical[56] and numerical[57] investigations, a droplet initially placed at the center-line of a channel flow, in the absence of a magnetic field, will translate only in the axial direction (*i.e.*, the x direction) for the viscosity ratio between dispersed and continuous phases $\lambda \lesssim 0.5$ or $\lambda \gtrsim 10$. In this work, $\lambda = \eta_f/\eta_o = 0.064$ and indeed the droplets are found to translate stably along the axial direction as shown in Fig. 2(a1)–(a3).

In the presence of a magnetic field, the droplet is deformed by the combination of shear and magnetic fields, the latter producing Maxwell stresses. Deformation due to shear is quantified by the capillary number $\mathrm{Ca} = \bar{u}\eta_o R_0/(\sigma w_c)$, while deformation due to

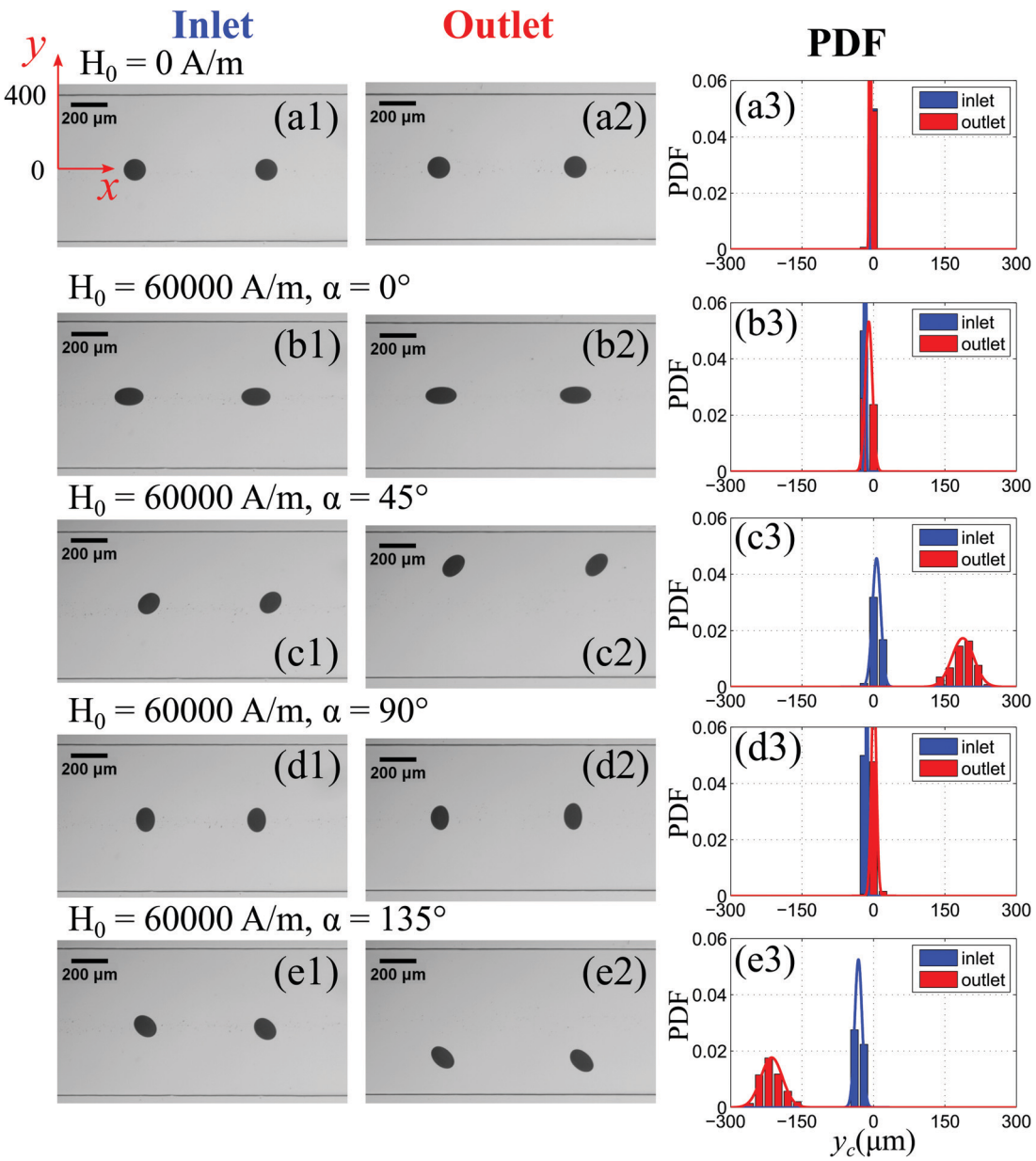

Fig. 2 Images of the inlet and the outlet, and the corresponding probability density function (PDF) of the centroid of the ferrofluid droplet in the y direction (a1–a3) without an applied magnetic field (H_0 = 0 A m^{-1}); (b1–b3) $H_0 \approx$ 60 000 A m^{-1}, and $\alpha = 0°$; (c1–c3) $H_0 \approx$ 60 000 A m^{-1}, and $\alpha = 45°$; (d1–d3) $H_0 \approx$ 60 000 A m^{-1}, and $\alpha = 90°$; and (e1–e3) $H_0 \approx$ 60 000 A m^{-1}, $\alpha = 135°$. The flow rates are Q_1 = 0.15 μL min^{-1}, Q_2 = 4.0 μL min^{-1} and Q_3 = 6.0 μL min^{-1} for all the experiments. The oil–ferrofluid interfacial tension σ = 4.31 ± 0.22 mN m^{-1}. Video clips for these experiments are available in the ESI.†

the magnetic field (assuming a linearly magnetizable material) is quantified by the magnetic bond number $\mathrm{Bo_m} = \mu_0 H_0^2 R_0/(2\sigma)$. In our experiments, Ca $\approx 7 \times 10^{-3}$ and $\mathrm{Bo_m} \approx 7$ suggest that the deformation due to the magnetic field is dominant.

This is borne out experimentally: we find that when a uniform magnetic field ($H_0 \approx$ 60 000 A m^{-1}) is applied along various directions, as shown in Fig. 2(b)–(e), the droplets become elongated in the direction of the magnetic field, with their elongation and orientation nearly independent of their position across the channel. Furthermore, we find that the direction of the magnetic field controls the direction of the cross-stream migration. When the magnetic field is parallel to the flow direction (*i.e.*, $\alpha = 0°$) as shown in Fig. 2(b1)–(b3), the droplets deform to achieve an ellipsoidal shape with their major axis parallel to the flow direction, and there is only a slight net lateral migration in the cross-stream direction, which might be attributed to the imperfection of the experimental conditions. As α increases to 45° as shown in Fig. 2(c1)–(c3), a similar deformed shape is observed and the elongation axis is aligned to 45°, which results in the droplet migrating towards the upper channel wall. The average distance of the cross-stream migration between the inlet and the outlet is measured to be 181.16 μm. When α increases to 90° as shown in Fig. 2(c1)–(c3), the elongation axis is perpendicular to the flow direction, and there is a slight net lateral migration in the

cross-stream direction (again this might be due to the imperfect control of the experiments). At an inclination angle $\alpha = 135^\circ$ as shown in Fig. 2(e1)–(e3), the elongation axis is aligned to 135°, which results in the droplets migrating towards the lower wall. The average distance of the cross-stream migration between the inlet and the outlet is −182.17 μm.

3.2 Cross-stream migration mechanism

The cross-stream migration of the droplet can be understood by considering hydrodynamic interactions between the droplet and the upper and lower walls of the channel. It is well known that the stresslet field around a droplet in shear flow alone, by hydrodynamic interactions with nearby boundaries, can result in a cross-stream migration of the droplet.[58] A key observation is that the component of the stresslet responsible for lateral migration depends on the inclination of the droplet's long axis relative to the flow. As discussed above, in our experiments, the droplet's orientation is set largely by the magnetic field, independent of the flow.

We estimate the cross-stream migration velocity by modeling the droplet as a rigid particle with a fixed orientation angle $\approx\alpha$ relative to the horizontal axis. Although this approximation neglects the influence of the interior flow of the droplet, it typically results in small errors in cases of shear-induced deformation.[56,59,60] The stresslet of the droplet can then be approximated using the relations of Kim and Karrila[61] for rigid ellipsoids. Next, we recognize that in the present experiments the droplet is centered between the channel walls in the depth direction, and therefore experiences shear gradients primarily in the width (y) direction. We introduce the Taylor deformation parameter $D = \frac{L-B}{L+B}$, where L and B are the semi-major and semi-minor axes, respectively, of the droplet; it should be noted that $0 \le D < 1$. Then, the yy component of the hydrodynamic stresslet is $S_{yy} = \eta_o \pi L^3 \partial_y u_x \left\{ \left(\frac{5}{6}X^M - \frac{5}{6}Z^M - 2Y^H\right) \sin 2\alpha . - \left(\frac{5}{4}X^M - \frac{5}{3}Y^M + \frac{5}{12}Z^M\right) \sin 4\alpha \right\}$, where X^M, Z^M, Z^M and Y^H are known functions of the deformation D (see Table 3.4 of Kim and Karrila ref. 61). The term proportional to $\sin 4\alpha$ is numerically much smaller than the term proportional to $\sin 2\alpha$ for the deformations measured in experiments, and is therefore neglected below. Accounting only for the first reflection of the stresslet with the upper ($y = w_c$) and lower ($y = 0$) walls, the cross-stream migration velocity of a droplet whose center is at a position $y_d \gg R_0$ is[58,62]

$$v_y \approx -\frac{9}{64\pi\eta_o}\left(\frac{1}{{y_d}^2} - \frac{1}{(w_c - y_d)^2}\right) S_{yy}\Big|_{y_d} \tag{1a}$$

$$\approx \frac{3{R_0}^3 \partial u_x}{7 \quad \partial y}\Big|_{y_d}\left(\frac{1}{{y_d}^2} - \frac{1}{(w - y_d)^2}\right)\frac{D}{1-D}\sin 2\alpha \tag{1b}$$

$$\text{for } D \ll 1,$$

Eqn (1b) is obtained as the leading term of a Taylor expansion of eqn (1a) for small deformations, although it remains accurate to within 10% even at $D = 0.5$.

The theoretical prediction (1b) quantitatively reproduces the direction of the vertical drift observed in the experiments: the droplet drifts towards the upper wall ($y = w_c$) for α in the first and third quadrants, and towards the lower wall ($y = 0$) for α in the second and fourth quadrants. Fig. 3 shows the comparison between the theory and the experiment when a droplet was under a magnetic field at $\alpha = 135^\circ$ and migrated towards the lower wall. It should be noted that $\partial u_x/\partial y$ in eqn (1) is determined using results (evaluated at the z-symmetry plane) for a rectangular channel,[63] and D is obtained from experimental measurements. According to the theory, the symmetry plane $y = 0$ is an unstable fixed point of the trajectory, so the droplet can, in practice, drift across it. This behavior is similar to recent theoretical predictions for the migration of droplets in Poiseuille flow under uniform electric fields.[64] Lateral migration due to both magnetic and electric fields is in contrast with the case of a droplet drifting due to deformation by shear flow alone, where the droplet migrates towards the centerline $y = w_c/2$, which in this case is a stable fixed point of the lateral migration dynamics when $\lambda \lesssim 0.5$ or $\lambda \gtrsim 10$.[56]

To further confirm the cross-stream migration mechanism of the droplet, a two-dimensional (2D) numerical model was

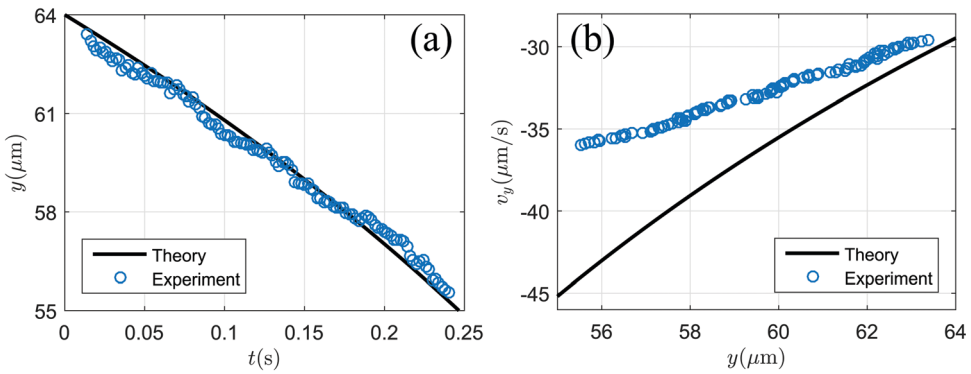

Fig. 3 Comparison of the cross-stream migration of a droplet close to the lower wall between the theoretical prediction and the experiment. (a) Vertical position of the particle (y) as a function of time. (b) Cross-stream velocity (v_y) as a function of y. Here the magnetic field is applied at $\alpha = 135^\circ$, and $D \approx 0.156$. It should be noted that the channel width is 300 μm.

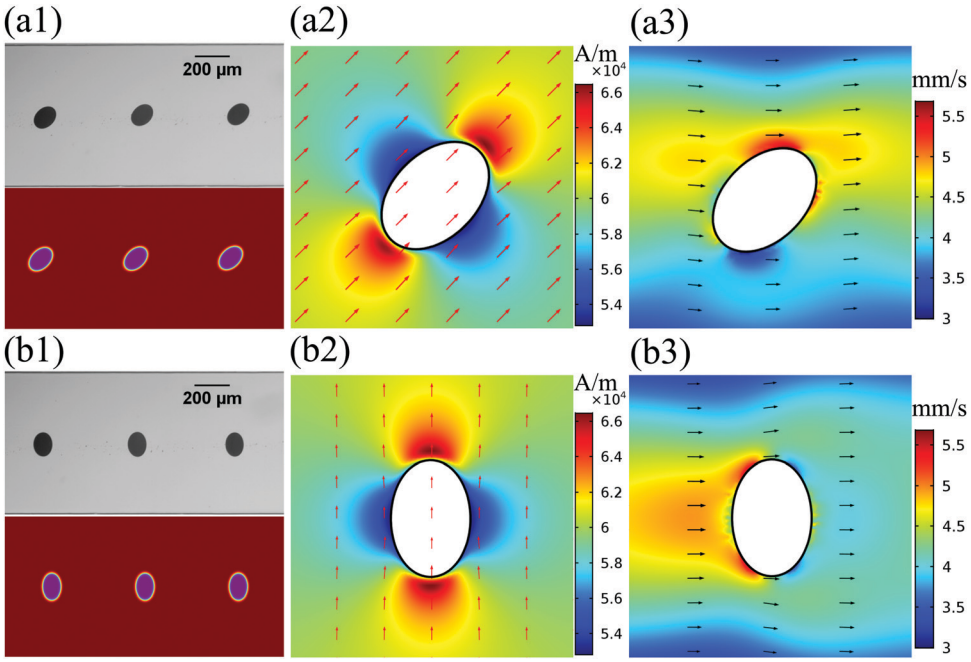

Fig. 4 (a) Comparison of the droplet trajectory between the experiments and the simulation (a1), and numerical results of the magnetic field (a2) and the velocity field (a3) for ferrofluid droplets when $\alpha = 45^\circ$. (b) Comparison of droplet trajectory between the experiments and the numerical simulation (b1), and numerical results of the magnetic field (b2) and the velocity field (b3) for ferrofluid droplets when $\alpha = 90^\circ$. The magnetic field strength $H_0 = 60\,000$ A m^{-1} and the oil–ferrofluid interfacial tension $\sigma = 4.31 \pm 0.22$ mN m^{-1}.

developed to investigate the ferrofluid droplet transport in the channel. By using a commercial finite element method solver (COMSOL Multiphysics), the numerical model employed the level-set method, and coupled the magnetic and flow fields. Briefly, the magnetic field is first determined by solving the magnetostatic equation, and the magnetic force term is then coupled to the Navier–Stokes equation. More details of the numerical modeling are available from our previous work.[65] The magnetic field with a strength of 60 000 A m^{-1} and a direction of 45° or 90° was used in the simulations.

Fig. 4(a1) shows a comparison of experimental and numerical results when the magnetic field is applied at $\alpha = 45^\circ$. As we can see, the numerical results are in quantitative agreement with the experiment. The magnetic field and the velocity field around the droplet are shown in Fig. 4(a2) and (a3). The magnetic force acting on the droplet is approximately zero for an ellipsoidal droplet placed in a uniform field,[50] which is supported by the numerical simulation of the magnetic field distribution (Fig. 4(a2)). The presence of magnetic fields leads to the generation of Maxwell stresses at the interface between the ferrofluid and olive oil, which causes the deformation of the droplet. Furthermore, the direction of elongation (*i.e.*, major axis) is aligned to the direction of the magnetic field. As a result of the ellipsoidal shape and the relative orientation of the droplet, the velocity profile around the droplet is asymmetric to the flow direction, as shown in Fig. 4(a3). This asymmetric orientation of the deformed droplet with respect to the flow direction results in the cross-stream migration towards the upper wall. It should be noted that at $\alpha = 135^\circ$, the droplet will move towards the lower wall.

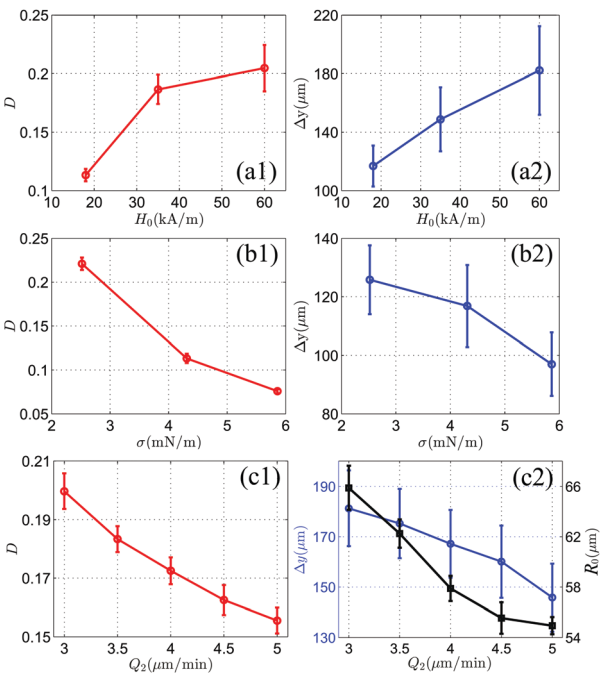

Fig. 5 Effect of magnetic field strength, interfacial tension and flow rates on droplet migration. (a) Taylor deformation parameter, D, and the net lateral migration, Δy, varying with magnetic field strength, H_0, when $\sigma = 4.31 \pm 0.22$ mN m^{-1}. (b) Taylor deformation parameter, D, and the net lateral migration, Δy, varying with interfacial tension, σ, when $H_0 \approx 18\,000$ A m^{-1}. (c) Taylor deformation parameter, D, the net lateral migration, Δy, and equivalent sphere radius, R_0, varying with flow rate, Q_2, when $H_0 \approx 35\,000$ A m^{-1}. The magnetic field is applied at $\alpha = 45^\circ$.

When applied at 90° to the flow direction, the magnetic field causes the droplet to deform to an ellipsoidal shape and the elongation direction is perpendicular to the flow direction. However, the velocity profile around the droplet is symmetric about the channel's centerline as can be seen from Fig. 4(b). Similarly, for $\alpha = 0°$, the droplet will be elongated parallel to the flow direction, and no cross-stream migration will take place either due to the symmetric flow field around the droplet. In both cases, the stresslet of the droplet is zero and therefore there are negligible hydrodynamic interactions with the walls.

3.3 Effects of magnetic field strength, interfacial tension and flow rate

As discussed earlier, the cross-stream migration depends on the deformation and relative orientation, which are expected to depend on the properties of the fluids, the flow field and the magnetic field. In a quiescent flow field, the deformation is related to the magnetic field strength, interfacial tension, and droplet size.[51] The droplet size depends on the flow rates used. So here, we focus on the effect of magnetic field strength, interfacial tension and flow rates on the drop migration by examining the case using a magnetic field applied at 45°, as shown in Fig. 5(a and b). We used the Taylor deformation parameter D to characterize the droplet deformation. From Fig. 5(a1), D increases with an increasing magnetic field, meaning the elongation of the ferrofluid droplet increases. The larger deformation causes a larger net lateral migration of the droplet as shown in Fig. 5(a2). Fig. 5(b) shows the effect of oil–ferrofluid interfacial tension on the drop migration when a magnetic field with $H_0 = 18\,000$ A m^{-1} is applied at 45°. As can be seen, D increases as the oil–ferrofluid interfacial tension decreases, resulting in increasing the net lateral migration of the droplet. When the flow rate Q_2 is adjusted, the droplet size changes as well. As can be seen in Fig. 5(c2), the equivalent radius, R_0, decreases with an increasing flow rate Q_2. This lowers the magnetic bond number, resulting in decreased deformation (Fig. 5(c1)) and smaller net lateral migration of the droplet.

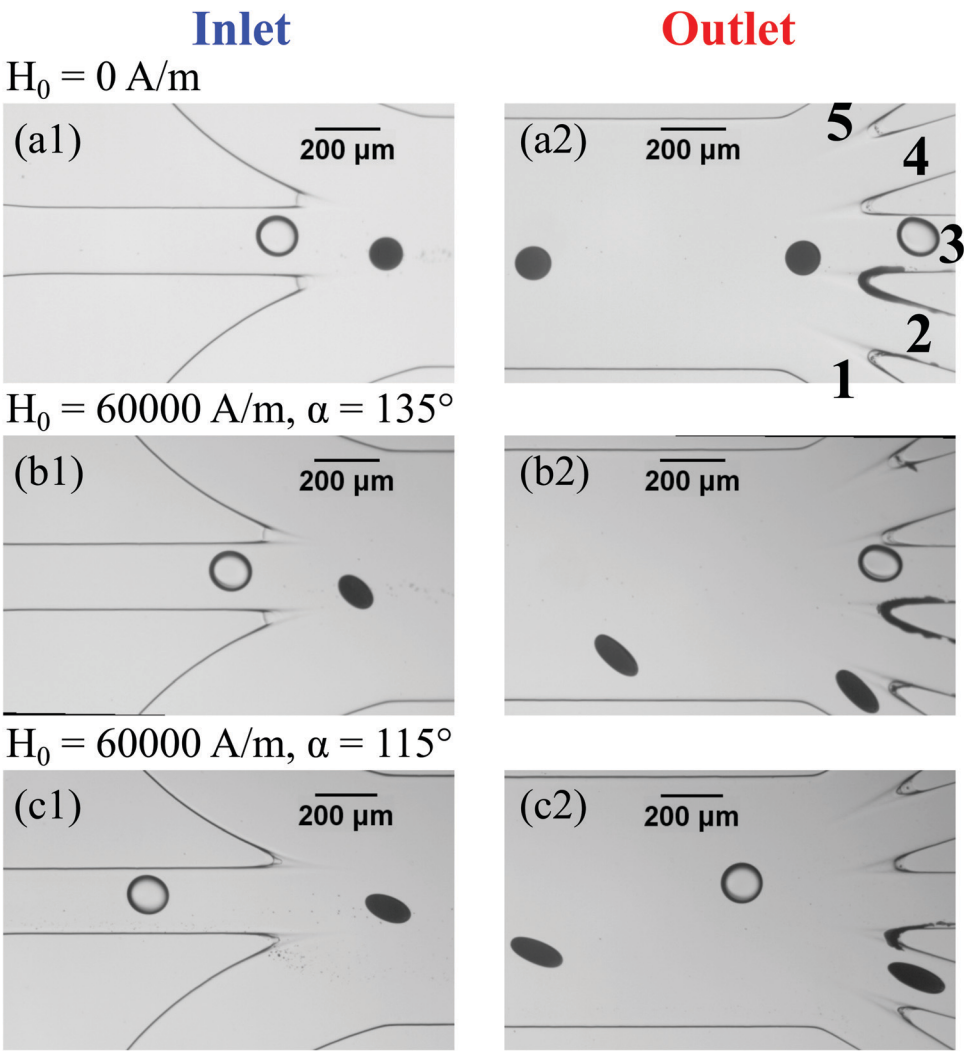

Fig. 6 The separation of ferrofluid and water droplets by a uniform magnetic field. (a) Both ferrofluid and water droplets flow into sub-microchannel 3 without a magnetic field; (b) the ferrofluid droplets flow into sub-microchannel 1 when $H_0 \approx 60\,000$ A m^{-1} and $\alpha = 135°$; (c) the ferrofluid droplets flow into sub-micrcahannel 2 when $H_0 \approx 60\,000$ A m^{-1} and $\alpha = 115°$. The oil–ferrofluid interfacial tension $\sigma = 2.52 \pm 0.22$ mN m^{-1}.

Therefore, we can see that the magnetic field strength, interfacial tension and the droplet size are three important factors for the migration of the droplet. The droplet deformation measured in the experiments is much smaller than those predicted by the existing theory[51] for a ferrofluid droplet in an unbounded fluid, which could be attributed to the confinement effect of the droplet.

3.4 Separation of ferrofluid and water droplets

The deformation-dependent migration under a uniform magnetic field can be used for selectively separating droplets that exhibit different deformations, which could be due to differences in size, interfacial tension, or magnetic properties. As an illustration, Fig. 6 shows the separation of ferrofluid droplets from water droplets by a uniform magnetic field. In this experiment, the ferrofluid and water droplets are all generated at the center of the channel. The oil–ferrofluid interfacial tension is $\sigma = 2.52 \pm 0.22$ mN m^{-1}. Without an applied magnetic field, both ferrofluid and water droplets flow into the center of sub-microchannel 3 and there is no separation, as can be seen from Fig. 6(a). When the magnetic field ($H_0 = 60\,000$ A m^{-1}) is applied at 135°, the water droplets remained at a similar initial position flowing into sub-microchannel 3, while the ferrofluid droplets moved to the lower wall and flow into sub-microchannel 1. Thus, complete separation is achieved. This magnetic manipulation is also tunable due to the easy control of the direction of the magnetic field. When the magnetic field is set at 115°, the ferrofluid droplets can be diverted to flow into sub-microchannel 2.

As has been described earlier, the droplet migration depends on the deformation and the orientation angle of the droplets; and the droplet deformation depends on the magnetic field strength, interfacial tension and droplet size. For fixed field strength and interfacial tension, the larger the droplet, the larger the deformation (it should be noted that the magnetic bond number scales with droplet radius). The current method will apply to micro-droplets as small as 10 microns, as long as the magnetic field is sufficiently strong. Under the conditions ($w_c = 800$ μm, $d_c = 70$ μm, $L = 13\,000$ μm, $H_0 = 60\,000$ A m^{-1}, $\sigma = 2.52$ mN m^{-1} and $Q_{total} = 10.15$ μL min^{-1}) used in this work, experimentally we find that the method can effectively manipulate droplets with radius larger than 70 μm.

4 Conclusions

In summary, we have demonstrated a unique approach to manipulate droplet migration in microfluidics by using a uniform magnetic field. In contrast to conventional magnetic manipulations, the current approach does not induce direct magnetic forces on the droplets. Instead, Maxwell stresses arise at the droplet interface due to a change in magnetic susceptibility across the droplet interface, and consequently deform the droplet and affect its relative orientation to the flow. Due to the deformed shape and the inclined angle to the shear flow, the droplet interacts hydrodynamically with the channel walls, and migrates in the cross-stream direction. We experimentally investigated various parameters that influence the droplet migration, including magnetic field strength, magnetic field direction and interfacial tension. It is found that the lateral migration speed increases with the droplet deformation, which in turn increases with the field strength and decreases with the interfacial tension. The magnetic field direction, on the other hand, controls the orientation of the drop and the direction of the lateral migration. The direction and speed of the lateral migration are well described by the hydrodynamic theory that accounts for the interactions of the droplet's stresslet flow with the walls of the channel. We have also developed a two-dimensional numerical model that predicts the lateral migration and confirmed negligible magnetic force.

In comparison to conventional magnetic separation, the uniform magnetic field technique is simple to implement and is favorable for high-throughput parallelization. Multiple microfluidic channels can be conveniently integrated onto a single chip while being subjected to the same uniform magnetic field. The demonstrated technique thus provides a general mechanism for the separation of micro-droplets, and has great potential for biological and biomedical applications that require sorting of droplets by their size, interfacial tension, or magnetic properties. One possible application would be sorting of biological cells that are encapsulated in ferrofluid droplets. Since the volume fraction of cells in a ferrofluid droplet would change the effective magnetic susceptibility, this change may lead to different deformation, lateral migration and separation of droplets.

Conflicts of interest

There are no conflicts to declare.

Acknowledgements

The authors gratefully acknowledge the support from the Department of Mechanical and Aerospace Engineering (MAE) and the Center for Biomedical Research (CBR) at the Missouri University of Science and Technology. This work is partially supported by the National Science Foundation (Grant No. DMS-1818642). BR acknowledges the Department of Mechanical Engineering and the Bourns College of Engineering at the University of California, Riverside for support.

Notes and references

1 M. T. Guo, A. Rotem, J. A. Heyman and D. A. Weitz, *Lab Chip*, 2012, **12**, 2146–2155.
2 N. Shembekar, C. Chaipan, R. Utharala and C. A. Merten, *Lab Chip*, 2016, **16**, 1314–1331.
3 G. Du, Q. Fang and J. M. den Toonder, *Anal. Chim. Acta*, 2016, **903**, 36–50.
4 L. Shang, Y. Cheng and Y. Zhao, *Chem. Rev.*, 2017, **117**, 7964–8040.
5 Y.-C. Tan, J. S. Fisher, A. I. Lee, V. Cristini and A. P. Lee, *Lab Chip*, 2004, **4**, 292–298.
6 Y.-C. Tan and A. P. Lee, *Lab Chip*, 2005, **5**, 1178–1183.

7 Y.-C. Tan, Y. L. Ho and A. P. Lee, *Microfluid. Nanofluid.*, 2008, **4**, 343.
8 A. C. Hatch, A. Patel, N. R. Beer and A. P. Lee, *Lab Chip*, 2013, **13**, 1308–1315.
9 E. Kadivar, S. Herminghaus and M. Brinkmann, *J. Phys.: Condens. Matter*, 2013, **25**, 285102.
10 T. Bowman, J. Frechette and G. Drazer, *Lab Chip*, 2012, **12**, 2903–2908.
11 H.-D. Xi, H. Zheng, W. Guo, A. M. Gañán-Calvo, Y. Ai, C.-W. Tsao, J. Zhou, W. Li, Y. Huang and N.-T. Nguyen, *et al.*, *Lab Chip*, 2017, **17**, 751–771.
12 D. R. Link, E. Grasland-Mongrain, A. Duri, F. Sarrazin, Z. Cheng, G. Cristobal, M. Marquez and D. A. Weitz, *Angew. Chem., Int. Ed.*, 2006, **45**, 2556–2560.
13 X. Niu, M. Zhang, S. Peng, W. Wen and P. Sheng, *Biomicrofluidics*, 2007, **1**, 044101.
14 B. Ahn, K. Lee, R. Louge and K. W. Oh, *Biomicrofluidics*, 2009, **3**, 044102.
15 B. Ahn, K. Lee, R. Panchapakesan and K. W. Oh, *Biomicrofluidics*, 2011, **5**, 024113.
16 F. Guo, X.-H. Ji, K. Liu, R.-X. He, L.-B. Zhao, Z.-X. Guo, W. Liu, S.-S. Guo and X.-Z. Zhao, *Appl. Phys. Lett.*, 2010, **96**, 193701.
17 L. Rao, B. Cai, X.-L. Yu, S.-S. Guo, W. Liu and X.-Z. Zhao, *AIP Adv.*, 2015, **5**, 057134.
18 L. Rao, B. Cai, J. Wang, Q. Meng, C. Ma, Z. He, J. Xu, Q. Huang, S. Li and Y. Cen, *et al.*, *Sens. Actuators, B*, 2015, **210**, 328–335.
19 K. Ahn, C. Kerbage, T. P. Hunt, R. Westervelt, D. R. Link and D. A. Weitz, *Appl. Phys. Lett.*, 2006, **88**, 024104.
20 J. J. Agresti, E. Antipov, A. R. Abate, K. Ahn, A. C. Rowat, J.-C. Baret, M. Marquez, A. M. Klibanov, A. D. Griffiths and D. A. Weitz, *Proc. Natl. Acad. Sci. U. S. A.*, 2010, 4004–4009.
21 R. de Ruiter, A. M. Pit, V. M. de Oliveira, M. H. Duits, D. van den Ende and F. Mugele, *Lab Chip*, 2014, **14**, 883–891.
22 A. Sciambi and A. R. Abate, *Lab Chip*, 2014, **14**, 2605–2609.
23 A. Sciambi and A. R. Abate, *Lab Chip*, 2015, **15**, 47–51.
24 D. J. Eastburn, Y. Huang, M. Pellegrino, A. Sciambi, L. J. Ptáček and A. R. Abate, *Nucleic Acids Res.*, 2015, **43**, e86.
25 L. Schmid, D. A. Weitz and T. Franke, *Lab Chip*, 2014, **14**, 3710–3718.
26 J. Nam, H. Lim, C. Kim, J. Yoon Kang and S. Shin, *Biomicrofluidics*, 2012, **6**, 024120.
27 S. Li, X. Ding, F. Guo, Y. Chen, M. I. Lapsley, S.-C. S. Lin, L. Wang, J. P. McCoy, C. E. Cameron and T. J. Huang, *Anal. Chem.*, 2013, **85**, 5468–5474.
28 F. Petersson, A. Nilsson, C. Holm, H. Jönsson and T. Laurell, *Lab Chip*, 2005, **5**, 20–22.
29 I. Leibacher, P. Reichert and J. Dual, *Lab Chip*, 2015, **15**, 2896–2905.
30 C. Lee, J. Lee, H. H. Kim, S.-Y. Teh, A. Lee, I.-Y. Chung, J. Y. Park and K. K. Shung, *Lab Chip*, 2012, **12**, 2736–2742.
31 N.-T. Nguyen, K. M. Ng and X. Huang, *Appl. Phys. Lett.*, 2006, **89**, 052509.
32 E. Surenjav, C. Priest, S. Herminghaus and R. Seemann, *Lab Chip*, 2009, **9**, 325–330.
33 K. Zhang, Q. Liang, S. Ma, X. Mu, P. Hu, Y. Wang and G. Luo, *Lab Chip*, 2009, **9**, 2992–2999.
34 D. Lombardi and P. S. Dittrich, *Anal. Bioanal. Chem.*, 2011, **399**, 347–352.
35 K. Zhang, Q. Liang, X. Ai, P. Hu, Y. Wang and G. Luo, *Lab Chip*, 2011, **11**, 1271–1275.
36 J. Kim, J. Won and S. Song, *Biomicrofluidics*, 2014, **8**, 054105.
37 B. Teste, N. Jamond, D. Ferraro, J.-L. Viovy and L. Malaquin, *Microfluid. Nanofluid.*, 2015, **19**, 141–153.
38 H. Li, Y. Wu, X. Wang, C. Zhu, T. Fu and Y. Ma, *RSC Adv.*, 2016, **6**, 778–785.
39 E. Brouzes, T. Kruse, R. Kimmerling and H. H. Strey, *Lab Chip*, 2015, **15**, 908–919.
40 G. Huang, M. Li, Q. Yang, Y. Li, H. Liu, H. Yang and F. Xu, *ACS Appl. Mater. Interfaces*, 2017, **9**, 1155–1166.
41 T. Neuberger, B. Schöpf, H. Hofmann, M. Hofmann and B. Von Rechenberg, *J. Magn. Magn. Mater.*, 2005, **293**, 483–496.
42 J. Gao, H. Gu and B. Xu, *Acc. Chem. Res.*, 2009, **42**, 1097–1107.
43 I. Torres-Daz and C. Rinaldi, *Soft Matter*, 2014, **10**, 8584–8602.
44 K. W. Oh and C. H. Ahn, *J. Micromech. Microeng.*, 2006, **16**, R13.
45 D. J. Laser and J. G. Santiago, *J. Micromech. Microeng.*, 2004, **14**, R35.
46 A. S. Lübbe, C. Alexiou and C. Bergemann, *J. Surg. Res.*, 2001, **95**, 200–206.
47 M. Hejazian, W. Li and N.-T. Nguyen, *Lab Chip*, 2015, **15**, 959–970.
48 Y. J. Sung, J. Y. H. Kim, H. I. Choi, H. S. Kwak and S. J. Sim, *Sci. Rep.*, 2017, **7**, 10390.
49 D. W. Inglis, R. Riehn, J. C. Sturm and R. H. Austin, *J. Appl. Phys.*, 2006, **99**, 08K101.
50 J. A. Stratton, *Electromagnetic theory*, John Wiley & Sons, 2007.
51 S. Afkhami, A. Tyler, Y. Renardy, M. Renardy, T. St. Pierre, R. Woodward and J. Riffle, *J. Fluid Mech.*, 2010, **663**, 358–384.
52 H. Raich and P. Blümler, *Concepts Magn. Reson., Part B*, 2004, **23**, 16–25.
53 Z. Zhang, R. Zhou, D. P. Brames and C. Wang, *Micro Nanosyst.*, 2015, **7**, 4–12.
54 R. Zhou, F. Bai and C. Wang, *Lab Chip*, 2017, **17**, 401–406.
55 A. Daerr and A. Mogne, *Journal of Open Research Software*, 2016, **4**, e3.
56 P.-H. Chan and L. Leal, *J. Fluid Mech.*, 1979, **92**, 131–170.
57 S. Mortazavi and G. Tryggvason, *J. Fluid Mech.*, 2000, **411**, 325–350.
58 J. R. Smart and D. T. Leighton Jr, *Phys. Fluids A*, 1989, **1**, 52–60.
59 G. I. Taylor, *Proc. R. Soc. London, Ser. A*, 1934, **146**, 501–523.
60 N. Aggarwal and K. Sarkar, *J. Fluid Mech.*, 2007, **584**, 1–21.
61 S. Kim and S. J. Karrila, *Microhydrodynamics*, Butterworth, 1991.
62 D. Matsunaga, F. Meng, A. Zöttl, R. Golestanian and J. M. Yeomans, *Phys. Rev. Lett.*, 2017, **119**, 198002.
63 N. A. Mortensen, F. Okkels and H. Bruus, *Phys. Rev. E: Stat., Nonlinear, Soft Matter Phys.*, 2005, **71**, 057301.
64 S. Mandal, A. Bandopadhyay and S. Chakraborty, *J. Fluid Mech.*, 2016, **809**, 726–774.
65 M. R. Hassan, J. Zhang and C. Wang, *Phys. Fluids*, 2018, **30**, 092002.

